Renewable Energy 90 (2016) 377–385

Contents lists available at ScienceDirect

Renewable Energy

journal homepage: www.elsevier.com/locate/renene

# Empirical and numerical analysis of small wind turbine aerodynamic performance at a plateau terrain in Kenya

David Wafula Wekesa [a, b, *], Cong Wang [a], Yingjie Wei [a]

[a] Institute of Dynamics and Control of Spacecrafts, School of Astronautics, Harbin Institute of Technology, Harbin City, PR China
[b] Department of Physics, Jomo Kenyatta University of Agriculture & Technology, Nairobi City, Kenya

ARTICLE INFO

*Article history:*
Received 28 February 2015
Received in revised form
3 November 2015
Accepted 1 January 2016
Available online 15 January 2016

*Keywords:*
Aerodynamic performance
SWT
CFD
WPD

ABSTRACT

Kenya's energy depends on fossil fuels and the country is yet to embrace alternative sources that are environmentally friendly. In this paper, empirical and computational approaches are presented to investigate aerodynamic performance of Small Wind Turbine (SWT) operation at arid rural Mwingi-Kitui plateau region, Kenya. We used empirical statistics to represent wind resource, and Computational Fluid Dynamics (CFD) to address SWT aerodynamic performance at the site. The numerical simulations, employing Transition Shear Stress Transport (SST) model and fully mesh resolved rotor, were performed and results obtained compared with empirical methods. From the Wind Power Density (WPD) values, 44.50–85.48 W/m$^2$ between turbine hub heights 20 and 60 m, the site corresponds to wind class ≈1; hence unsuitable for grid-connected power generation. In addition, the numerical findings give useful insights to SWT aerodynamic performance with respect to empirical approach at a plateau terrain wind regime.



## 1. Introduction

Energy remains the major resource to transform a developing country into a developed one [1–4]. Kenya is a developing country, with energy mainly derived from woody biomass (68%), Petroleum fuels (22%), and electricity (9%) [5]. These competing energy sources have impacted negatively on the environment. In addition, electricity, which is mainly hydro-power driven, is highly unreliable. This is attributable to persistent droughts with consequential drying of water reservoirs [5]. Despite the country's struggle to solve energy challenges, like establishing plants driven by geothermal and diesel generators, energy cost continued to rise in the last decade.

On average, National surveys have revealed that almost 90% of Kenyans rely on traditional fuels such as biomass, charcoal, and dung to meet their heating and cooking needs. Dependence on firewood in the rural areas as the main source of cooking fuel is on the rise, with more than 80% of households relying on firewood for cooking compared to 10% of urban households. Charcoal is the second most popular type of cooking fuel used by 13.3% of households, while Kerosene is the third and frequently utilized among 44.6% of urban dwellers [6].

To reverse the trend of over dependence on fossils fuels, as well as enhance access to cheap and reliable energy, there is need for the country to diversify its energy sources. In addition, new technologies to harness local resources should be embraced to generate energy. This will support economic development and promote self-sufficiency in energy needs with emphasis to the rural poor population [5]. Wind energy is the latest veritable alternative energy source that is renewable for power production over the last decade, and offers the potential for $CO_2$ emissions reduction in power generation [7–9]. For global $CO_2$ emissions reduction to be realised, power generation should strongly depend on utilizing renewable energy systems, especially in the developing countries.

However, effective use of wind energy requires precise wind energy resource assessment. Precise wind speed measurements plays an important role for estimating the wind energy potential of a target site. Generally, wind resource assessment includes [10–12]: onsite wind conditions measurement; correlations between onsite meteorological towers to fill in missing data; correlations between long-term weather stations and short-term onsite meteorological towers; analysis of the wind shear and its variations; modelling of the distribution of wind conditions, and

* Corresponding author. Institute of Dynamics and Control of Spacecrafts, School of Astronautics, Harbin Institute of Technology, Harbin City, PR China.
*E-mail addresses:* dwekesahit@gmail.com (D.W. Wekesa), alanwang@hit.edu.cn (C. Wang), weiyingjie@gmail.com (Y. Wei).

http://dx.doi.org/10.1016/j.renene.2016.01.004
0960-1481/

prediction of the available energy at the site.

In Kenya, there is need for prospective and utilization of wind energy resource as a solution to provision of sustainable, reliable and cost effective power to the rural areas and urban poor. One of the main challenge to exploitation of wind energy resource can be attributed to non-availability of the wind resource data in the rural areas where the bulk of the country's population (84%) resides [13]. Currently, the country has 34 national meteorological stations centred in national airports and airstrips in urban areas [14]. However, their data is gathered at meteorological height of 10 m and is intended for agro-meteorology and civil aviation and hence not specific for harnessing wind as a source of energy [5,14]. Thus, in order to supply the increasing demand for the production of electricity especially for remote application, SWTs have an effective role [15].

Based on the 6 years data collected from four meteorological stations in Hong Kong, He et al. [16] investigated a surface wind characteristics with different terrain conditions. Wind turbulent characteristics under different terrains were compared based on long-term field measurements. From the study in Ref. [16], wind characteristics which determine wind energy potential of a site, can be significantly affected by surrounding terrains or topographies. Therefore, different upwind terrain or topographical conditions may result in remarkably varied distributions of local wind resource and hence wind energy potential of a region. Similar observations have been made in related studies in Refs. [1,17–24].

Using empirical methods, Mukulo et al. [5] and Kamau et al. [25] have analysed the wind energy potential for Marsabit and Mwingi-Kitui plateau, respectively, both Eastern regions of Kenya. Despite the empirical methods being prone to many statistical errors, with limitation in both time and cost, the studies results are very useful to wind energy technology stakeholders [26]. However, unsteady phenomena in the plateau terrains due to SWT rotational aerodynamics cannot be investigated by classical tools, such as empirical and Blade Element Momentum (BEM) methods.

Therefore, in the present study, we seek to employ both empirical and CFD approaches to evaluate aerodynamic performance of SWT operation at a remote power-starved population in rural Kenya. The results presented in this paper show that turbine hub height elevation has a very predictable influence on SWT aerodynamic performance through its effect on air density and kinematic viscosity. In addition, the numerical results provides detailed understanding of CFD application and its added value in evaluating SWT aerodynamic performance with respect to empirical approach at a plateau terrain.

## 2. Methodology

### 2.1. Experimental techniques

Following the empirical study by Mukulo et al. [5], wind speed measurements were performed at a tower height level of 20 m, located at the Mwingi-Kitui plateau, Kenya. The plateau terrain site is geographically located at an altitude of 0517 m above sea level on latitude $1.00^0$ S and longitude $38.01^0$ E. Wind speed data were measured every 10 s and averaged at intervals of 10 min for storage in a data logger. The 10 min averaged wind speed data were further averaged over an hour and stored sequentially in a permanent memory for a period of 12 months. Furthermore, the wind speed at higher heights of 40 m, 60 m, 80 m, and 100 m could be calculated using the power law (Eq. (1)). The annual mean wind speeds for turbine hub heights were used as $U_{mean}$ of fluctuating wind, while respective standard deviations ($\sigma_s$) averages as fluctuation amplitude $U_{amp}$ to represent the wind characteristics of the site [27].

The wind profile power law is a relationship between the wind speeds at one height, and those at another. It is often used in wind power assessments where wind speed data at various heights must be adjusted to a standard height prior to use. The wind power law was used to convert the measured wind speed at 20 m elevation to higher heights as in the case of an empirical study in Ref. [5]. The power law is expressed as:

$$v_z = v_1 \left(\frac{z}{z_1}\right)^{\alpha}, \tag{1}$$

where $v_z$ is the wind speed at height $z$ and $v_1$ is the reference wind speed at the reference height $z_1$. The exponent $\alpha$ is an empirically derived coefficient that depends on such factors as surface roughness and atmospheric stability [28]. The value of the empirical exponent varies from less than 0.10 for very flat land, water or ice to more than 0.25 for heavily forested landscapes and typical value of 0.14 for low roughness surfaces [2]. The value of 0.20 for exponent has been chosen to describe the actual nature of ground cover at the site. The empirical power law exponent of 0.20 fits within the description of the American Wind Energy Association (AWEA) for a site with short grass, hedges and few trees which best describes the plateau terrain at the site [5].

#### 2.1.1. Optical encoders

An optical encoder transducer was used to generate coded reading of measurement. Shaft encoders were used for measuring angular displacement and velocity. The anemometer and wind vane sensors in this study were developed using the incremental and absolute encoders, respectively, to generate digital signals. Advantages of digital transducers over analogue ones include high resolution, high accuracy, and relative ease of adaptation in digital control systems. Details of the experimental setup involving calibration of wind sensors have been discussed in previous wind assessment studies by the authors in Wekesa et al. [28,29].

#### 2.1.2. Measuring wind speed and direction

The wind sensors were clamped on a horizontal metallic support masked on a strong metallic vertical stand 20 m above the surface. The wind sensors were separated well enough to avoid the flow disturbance due to the blowing wind. The signals from both anemometer and wind vane sensors were fed to CR 10 Campbell microcontroller-based data logger. Wind data was measured and stored in the Electrically Erasable Programmable Read-Only Memory (EEPROM). Reading of wind speed was done at interval of 3 times a day alongside conventional instruments at the meteorological station for comparison. The language used by the data logger is C which is a general-purpose programming language that can work on any Automatic Voltage Regulator (AVR) microcontrollers. Detailed description of the software design and high resolution data logging instrumentation system for wind speed and direction measurement can be found in Wekesa et al. [28,29]. The data logging system flow chart is as shown in Fig. 1.

#### 2.1.3. Accuracy of measurements

A linear regression fit chart was used to test and establish a correlation between the wind speed data by Mukulo et al. [5] meteorological anemometer with calibrated mast-mounted optical anemometer. The results of the comparison between two anemometer measurements are displayed in the time series and scatter diagram shown in Fig. 2. The figure shows a very good correlation between the data obtained by Mukulo et al. [5] meteorological anemometer with those of the experimental mast-mounted optical anemometer. Therefore, Mukulo et al. [5]

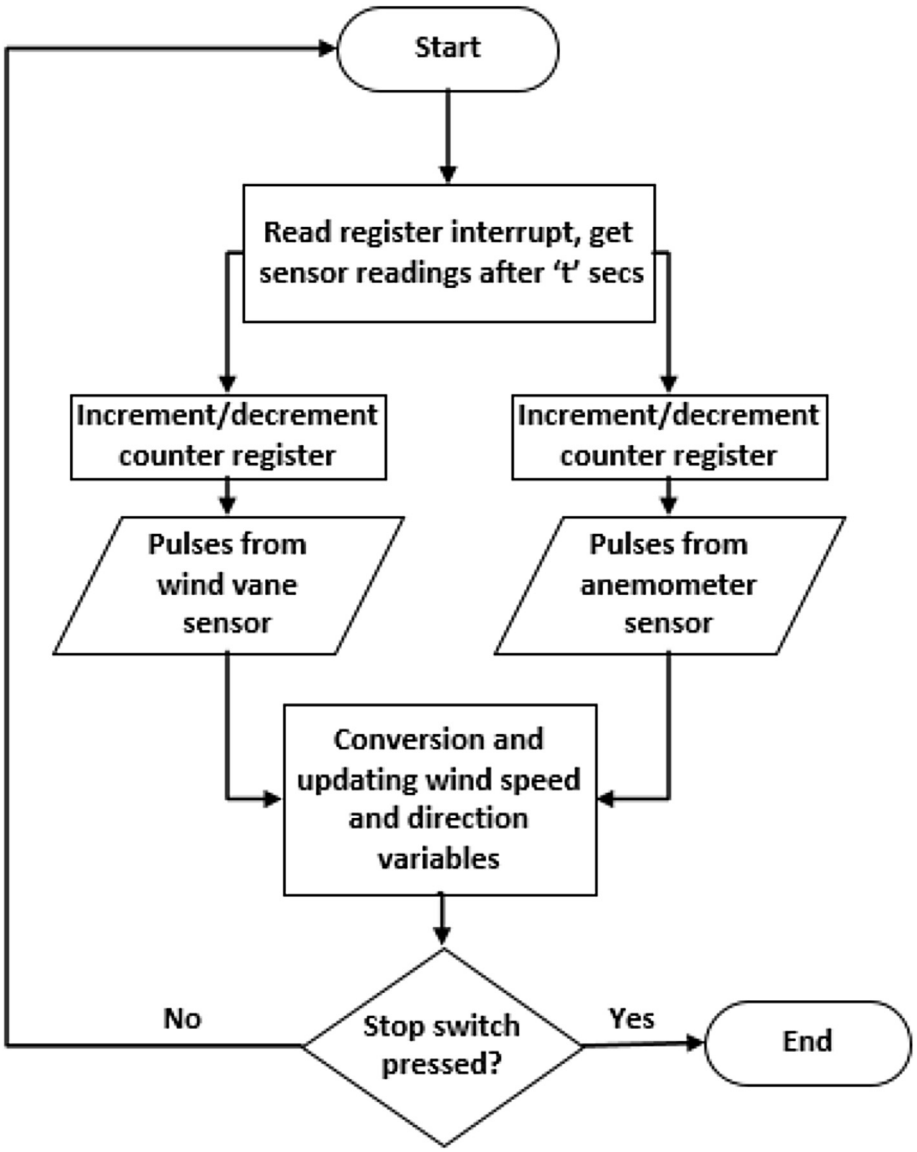


**Fig. 1.** Data logging system flow chart.

wind data measurement is reliable to predict long term pattern of wind regime. Furthermore, the strong correlation confirms that the experimental anemometer gives the correct readings and practical readings can be approximated to the data from the meteorological station.

Furthermore, Mukulo et al. [5] obtained specific data for harnessing wind resource at the site, and it was also revealed that most of the plateau terrain wind had mean speeds between 4 and 7 m/s. Observe from the wind speed frequency distribution in Fig. 3 that, the mean wind speed frequency ranged between 10 and 25% although in a small percentage. Most of the study months depicted absence of both very low wind speeds between 0 and 2 m/s as well as very high wind speeds (>9 m/s). From the wind speed frequency distribution (Fig. 3), the most frequent wind speed is 5.5 m/s flowing for 25% of the total time in a year with usable quality wind (above 3.5 m/s) available for above 80% of the total study time. The annual averages of shape k (dimensionless) and scale c (m/s) parameters of the Weibull distributions were 3.54 and 5.45 m/s respectively [5].

### 2.2. Numerical techniques

#### 2.2.1. The flow solver

There are three main forms of turbulence simulation methods adopted in the CFD community, i.e. Direct Numerical Simulation (DNS), Large Eddy Simulation (LES), and Reynolds-Averaged Navier–Stokes (RANS) [30–34]. Although DNS method is among advanced computational approaches in which all the space and time scales are resolved, it requires a large amount of computing resources and time. The LES method is appropriate for 3D simulations hence still very computationally expensive to numerically investigate the complex unsteady dynamics phenomenon due to the 3D nature of the eddies [35–37]. Recently, more advanced CFD models are available, solving both three-dimensional (3D) and two-dimensional (2D) Navier–Stokes equations for wind turbine aerodynamics modelling [26,38–42].

Based on studies in Refs. [26,27,43], it has been shown that a 2D model is sufficient enough in predicting the performance and aerodynamics that surround the Vertical Axis Wind Turbine

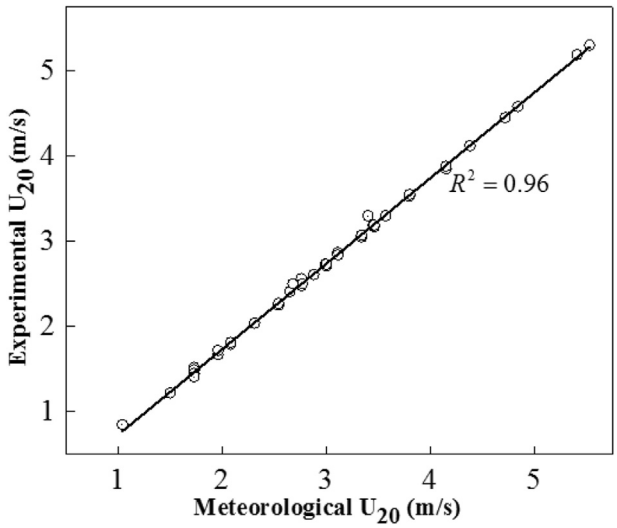


**Fig. 2.** Linear regression fit at a height of 20 m.

(VAWT). In the present study, a 2D CFD model has been used to represent the virtual wind tunnel; and unsteady RANS approach appears to be the most suitable to predict the aerodynamic performance simulations with an acceptable computational cost and, at least, reasonable accuracy. Therefore, a 2D incompressible unsteady CFD solver, based on finite volume method in the commercial software package ANSYS® Fluent®, is employed to solve the full unsteady RANS governing Eqs. (2) and (3):

$$\frac{\partial u_i}{\partial x_i} = 0, \tag{2}$$

$$\frac{\partial u_i}{\partial t} + u_j \frac{\partial u_i}{\partial x_j} = -\frac{1}{\rho}\frac{\partial p}{\partial x_i} + \nu \frac{\partial^2 u_i}{\partial x_j \partial x_j} - \frac{\partial \overline{u_i' u_j'}}{\partial x_i}, \tag{3}$$

where, $i, j = 1, 2$. Here $x_1$ and $x_2$ denote the horizontal and vertical directions, respectively; $u_i$ and $u_j$ are the corresponding mean velocity components; $t$ is the time; $\rho$ is the density of the fluid; $p$ is the dynamic pressure; $\nu$ is the kinematic viscosity; and $\overline{u_i' u_j'}$ is the Reynolds stress component where $u_i'$ denotes the fluctuating part of the velocity. The reader is referred in Refs. [26,32,44,45] for detailed description about unsteady RANS approach formulation.

### 2.2.2. Computational domain and solution methodology

The CFD computational domain consists of two mesh zones; the inner circular Rotor sub-grid zone and the rectangular outer zone. The two zones communicate via a pair of circular interfaces between them. To this end, a User-Defined Function (UDF) subroutine is developed and attached to the flow solver to control the dynamic mesh motion. The inner Rotor sub-grid zone is composed of three symmetric airfoil blades rotating at a common angular velocity. The three airfoil blades are spaced equally at 120° apart as shown in Fig. 4. The blades were defined as no-slip walls, while both interface boundary of the Rotor sub-grid and the outer rectangular wind tunnel sub-grid were set as an interface. No-slip wall boundary condition is used in this simulation to model the bottom and the top sides of the domain as was the case in Refs. [26,31].

From the wall distance study by Danao et al. [31], the side wall distance was set to 1.2 m from SWT axis test section (Fig. 4). The velocity inlet boundary condition from the test section was set to 1.5 m, 0.3 m short of the 1.8 m in Wekesa et al. [26,27]. Since the modelled turbulence intensity decay in the simulations matched that of the experiments, this was not considered important. Like the case in Refs. [26,27], the pressure outlet boundary condition was set to 3 m downwind to match the actual distance of the wind tunnel fan from the SWT axis of rotation [46]. The reader is referred to [ [26,27,31,47,48], and references therein] for full details on domain boundary location with both mesh and time step independence preliminary studies.

Following blade thickness analysis study in Wekesa et al. [27], the airfoil coordinates of a National Advisory Committee for Aeronautics (NACA) 4-digit (00XX) series symmetric profile of NACA 0022 were imported to define the blade shape. A moving mesh approach with a sliding mesh technique was used for the rotation of the inner circular Rotor sub-grid zone in order to capture the torque generated by the three blade airfoils [26].

From Fig. 4(b), the inner circular Rotor sub-grid zone coincides exactly with the circular opening within the outer stationary rectangular zone. The interface of the two mesh zone boundaries slide against each other with no excessive overlap to minimize numerical diffusion, and have approximately the same characteristic cell size in order to obtain faster convergence [26,31,43].

The mesh was based on structured O-grid topology where the size of the first cell height next to the wall was such that the $y^+$ values from the flow solutions did not exceed 1 [49]. This was the limit of the turbulence model that was chosen for the simulations. The O-type mesh was primarily used in preference to conventional C-grid topology because the expected wake is not fixed on a specific path relative to the blade; but rather varying greatly in direction swaying from one side to another side [26,31,50].

The coupled pressure-based solver was chosen with a second order implicit transient formulation for improved accuracy to solve low-speed incompressible flows. All the governing equations for the solution variables, which are decoupled from each other, are solved sequentially. The Semi-Implicit Method for Pressure-Linked Equations (SIMPLE) algorithm is applied as the pressure–velocity

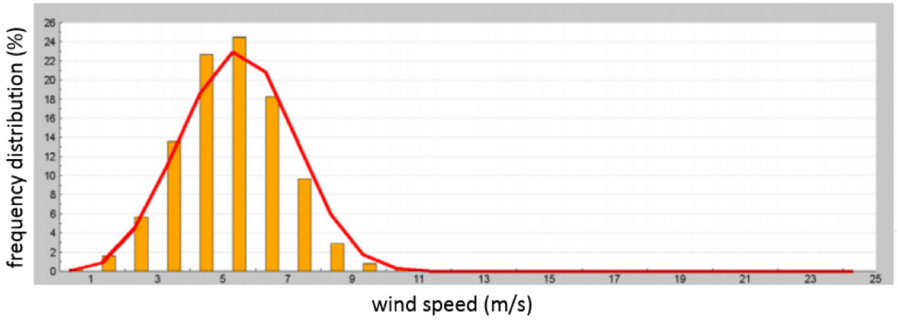


**Fig. 3.** Wind speed frequency distribution within plateau regime for one year [5].

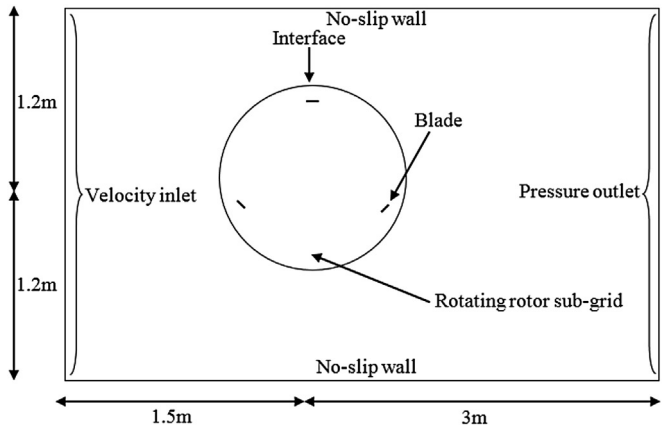


(a) Schematic representation of 2D numerical domain

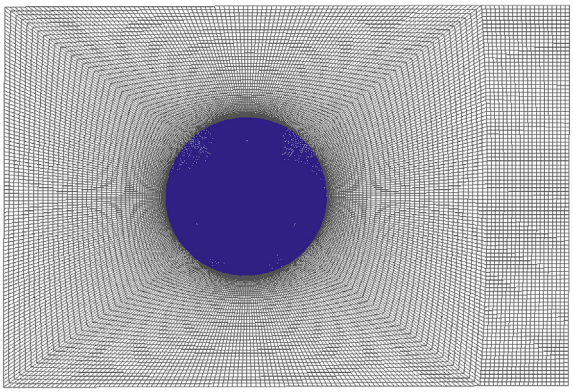

(b) Rotating inner and stationary outer domain meshes

**Fig. 4.** An illustration of boundary conditions and meshes of the 2D numerical domain.

coupling algorithm. With respect to the discretization of the convection terms in the transport equations for the velocity and turbulence quantities, second-order upwind schemes are utilised [31,32].

The Green-Gauss cell based method has been employed for calculating the gradients of the transport quantities on the faces of the cell boundaries. The under-relaxation factors are imposed to avoid numerical instabilities in the solution and their details are reported in Table 1. The turbulence intensity of inlet flow is set to 11% with a turbulence viscosity ratio of 14. These conditions and the complete validation of the present numerical code is based on an empirical study illustrated by Mukulo et al. [5] at the site.

The present simulations required an average of about 20 sub-iterations to make the solution converge at each physical time step. The time step convergence was monitored and the simulation was considered to have converged when residuals of all conserved variables fell below $1\times10^{-5}$ [26,27,43]. The calculations were performed on a computer having, Intel® Core™ i7-2600 CPU@3.40 GHz, 4 cores, 8 threads, physical RAM of 8 GB, and Windows 8 professional 64-bit operating system. Each simulation required a total Central Processing Unit (CPU) time of about 4 days. The details of the numerical set-up are reported in Table 2 for easier comparison with other numerical experiments.

The Transition SST model was used for turbulent calculations, as suggested from recent studies by Wekesa et al. [26,27]. This was attributable to its well behavior in adverse pressure gradients and separating flow, which were typically seen during the unsteady wind inflow operation on a turbine rotor scale. In addition, the Transition SST turbulence model has shown a close positive performance prediction for simulating SWT transient flows [31,51,52]. Detailed explanation for the turbulence model preliminary studies including the assumption made can be obtained in [[26,27,31,47,48], and references therein]. Therefore, the Transition SST model was employed for all the successive numerical simulations in this study.

**Table 1**
Under-relaxation factors.

| | | |
|---|---|---|
| Pressure | 0.2 | [−] |
| Density | 1 | [−] |
| Body forces | 1 | [−] |
| Momentum | 0.7 | [−] |
| Turbulent kinetic energy | 0.8 | [−] |
| Specific dissipation rate | 0.8 | [−] |
| Intermittency | 0.8 | [−] |
| Momentum thickness Re | 0.8 | [−] |
| Turbulent viscosity | 1 | [−] |

## 3. Results and discussion

In the present study, five angular velocities are tested, ranging from 55.73 rad/s to 77.28 rad/s with free-stream wind velocities $U_\infty$ from 4.24 m/s to 5.88 m/s. The corresponding turbine hub height elevation range was from 20 m to 100 m in increments of 20 m, respectively.

### 3.1. Small wind turbine aerodynamic performance

The calculated values of wind power density (wind power production per square area of a turbine) by the numerical method were compared with those of the empirical study in Ref. [5]. Higher hub heights were used to give higher wind power densities for practical small-scale harnessing of wind energy. The numerical power performance for the plateau site at various turbine hub heights above ground level is summarized in Table 3. The calculated numerical blade average power $P_B$ and wind average power $P_w$ ranges from 3.06 to 15.26 W and 47.04–81.16 W at 40 m–100 m turbine hub heights, respectively. However, at the lowest turbine hub height of 20 m, numerical $P_B$ and $P_w$ are −0.27 W and 31.15 W, respectively, resulting into a negative power coefficient of −0.01. The largest positive CP performance of 0.19 is registered at 100 m turbine hub height with a highest prevailing mean wind speed of 5.88 m/s. This is attributable to shorter bursts of high speed winds (gusts) occurring between the normal wind flow speeds ranging between 8 and 10 m/s [5,27]. The averaged numerical wind power density WPD as a function of $P_w$ over one wind cycle divided by SWT projected area A, defined as

$$WPD_{numerical} = \frac{P_w}{A} = \frac{1}{2}\rho U_\infty^3, \tag{4}$$

matches the empirical wind power densities at all turbine hub height elevations, hence confirming the reliability of the results.

From Fig. 5, both wind power densities varied uniformly across

**Table 2**
Details of the numerical set-up.

| Description | Value |
|---|---|
| Air kinematic viscosity [$m^2/s$] | $1.8\times10^{-5}$ |
| Air mass density [$kg/m^3$] | 1.132 |
| Angular velocity [rad/sec] | 55.73–77.28 |
| Free-stream wind velocity [m/s] | 4.24–5.88 |
| Machine mean tip speed ratio [−] | 4.6 |

**Table 3**
Numerical power performance.

| Hub height of turbine (m) | 20 | 40 | 60 | 80 | 100 |
|---|---|---|---|---|---|
| Mean wind speed $U_{mean}$ (m/s) | 4.24 | 4.88 | 5.30 | 5.62 | 5.88 |
| Fluctuating amplitude $U_{amp}$ (m/s) | 0.61 | 0.56 | 0.53 | 0.45 | 0.41 |
| Power coefficient CP | −0.01 | 0.07 | 0.13 | 0.15 | 0.19 |
| Blade average power $P_B$ (W) | −0.27 | 3.06 | 7.65 | 11.04 | 15.26 |
| Wind average power $P_w$ (W) | 31.15 | 47.04 | 59.83 | 71.23 | 81.16 |

the turbine hub heights with the numerical power density curve revealing slightly higher WPD. This can be attributed to the fact that 2D vertical axis SWT models are essentially SWTs with infinite blade aspect ratio AR which shifts the numerical power density upwards, but the general shape is maintained [27,31,52,53].

Table 4 shows numerical and empirical power densities at five turbine hub heights with characteristic fluctuating amplitudes at respective fluctuating mean wind speeds. The air density $\rho$ for the plateau terrain based on temperature and height above sea level is 1.132 kg/m$^3$ [5]. Furthermore, from Table 4, the minimum to maximum empirical WPD range falls within that of the numerical WPD range across the turbine hub heights.

Fig. 6 shows numerical power performances ($P_B$, and $P_w$) across the five turbine hub height elevations for the plateau terrain site. The available power in the wind increases with rising free-stream velocity $U_\infty$ up to the maximum peak values generated within the first half cycle of the wind cycle at all turbine hub heights. Afterwards, wind power plummets to its minimum value at all turbine hub height elevations in the second half of the wind cycle. In the plateau wind condition under study, a total of 9, 10.5, 11, 12, and 12.5 rotor rotations completes one periodic wind cycle for fluctuating mean wind speeds $U_{mean}$ at hub heights 20, 40, 60, 80, and 100 m, respectively. A detailed description and notations on the number of rotor rotations allowed to capture periodic convergence in one full wind cycle of fluctuation has been discussed in previous studies by the authors in Wekesa et al. [26,27].

In addition, from Fig. 6, the maximum $P_w$ peaks are 45.20, 63.78, 78.51, 88.61, and 98.60 W for turbine hub heights 20, 40, 60, 80, and 100 m, respectively. These corresponds to maximum wind power density peaks of 64.57, 91.11, 112.16, 126.59, and 140.86 W/m$^2$ (refer to Eq. (4)). Therefore, as was observed in Refs. [27,46], the performance of a turbine in a fluctuating wind follows the wind velocity

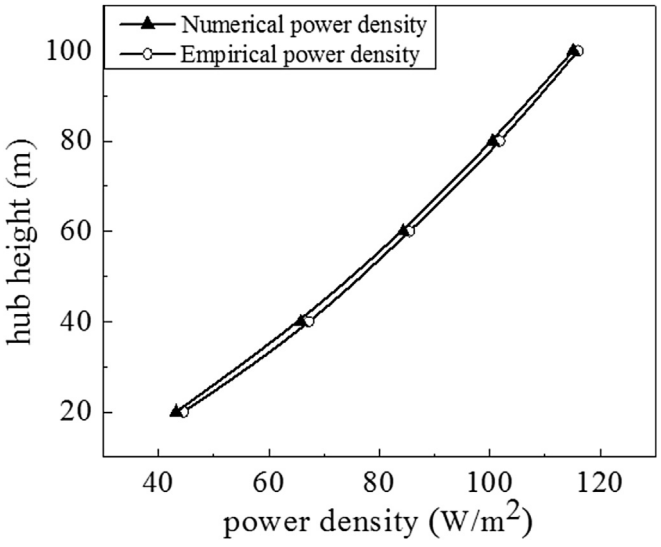


**Fig. 5.** Turbine hub height versus wind power density.

**Table 4**
Empirical and numerical wind power density.

| Hub height (m) | $U_{mean}$ (m/s) | $U_{amp}$ (m/s) | Wind power density (W/m$^2$) | |
|---|---|---|---|---|
| | | | Numerical | Empirical |
| 20 | 4.24 | 0.61 | 44.50 | 43.2 |
| 40 | 4.88 | 0.56 | 67.21 | 65.8 |
| 60 | 5.30 | 0.53 | 85.48 | 84.3 |
| 80 | 5.62 | 0.45 | 101.75 | 100.5 |
| 100 | 5.88 | 0.41 | 115.95 | 115.1 |

variations.

The wind power performance is further analysed in Fig. 7, showing the distribution of the instantaneous power coefficient CP (rot),

$$CP(rot) = \frac{P_B}{\frac{1}{2}\rho A U_\infty^3}, \tag{5}$$

as a function of rotor rotation for the SWT across the five hub heights. The blade average power $P_B$ is obtained from computing average of instantaneous blade power for the three rotor blades over the periodic wind cycle at each turbine hub height elevation.

From Fig. 7, the unsteady plateau wind CP and quasi-steady CP are presented using moving average smoothing method as the wind fluctuates at various turbine elevations. Smoothing the unsteady CP is necessary as it provides comparative plots of CP performance across the various fluctuating wind speeds at different turbine hub heights in the plateau environment. Furthermore, smoothing is shown to be consistent with the cycle-averaged method of computing for the rotor CP in steady wind conditions [27,31]. Hence, the fluctuating nature of the blade torque is filtered to give a single value of prediction of SWT aerodynamic performance.

The unsteady plateau wind CP summary in Table 3 is revealed in more detail in Fig. 7 where the quasi-steady positive CP is registered across the turbine hub heights, except for 20 m turbine hub height elevation with a fluctuating mean wind speed of 4.24 m/s. The results are in agreement to an empirical study by Mukulo et al. [5] at the site where positive wind performance was projected at hub heights above 40 m. Following the low wind power density values (Table 4), 44.50–85.48 W/m$^2$ between turbine hub heights 20 and 60 m, the plateau region corresponds to wind class ≈1. Similar details on wind power classification were revealed by Kamau et al. [25] and National Renewable Energy Laboratory (NREL) [54] where wind power class ≈1 represented WPD range between 0 and 200 W/m$^2$ at 50 m turbine hub height elevation. Consequently, the plateau region is considered unsuitable for grid connected power generation.

It is noteworthy that, in practice, the hub heights of small wind turbines are certainly lower and cannot be installed at high towers (20–100 m), because they are typically designed to be used in urban wind environment. Therefore, wind speed calculation at very high turbine hub heights, 20–100 m, was performed to specifically show CFD numerical approach in addressing SWT aerodynamic performances and its added value with respect to the empirical approach, rather than exploring site's suitability based on the SWT use.

## 4. Conclusion

In this study, the empirical and numerical approaches have been employed to evaluate aerodynamic performance of small wind

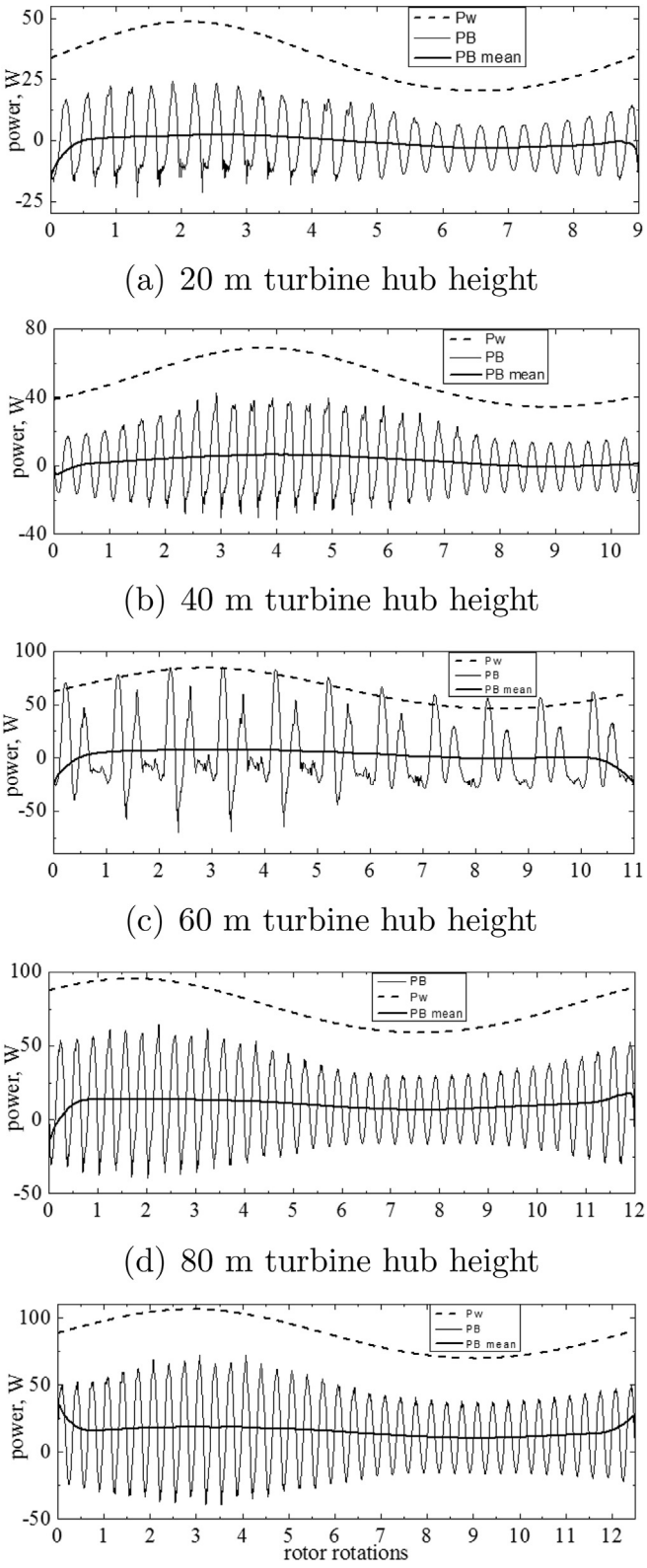


**Fig. 6.** Power performances ($P_B$ and $P_w$) at different turbine elevations.

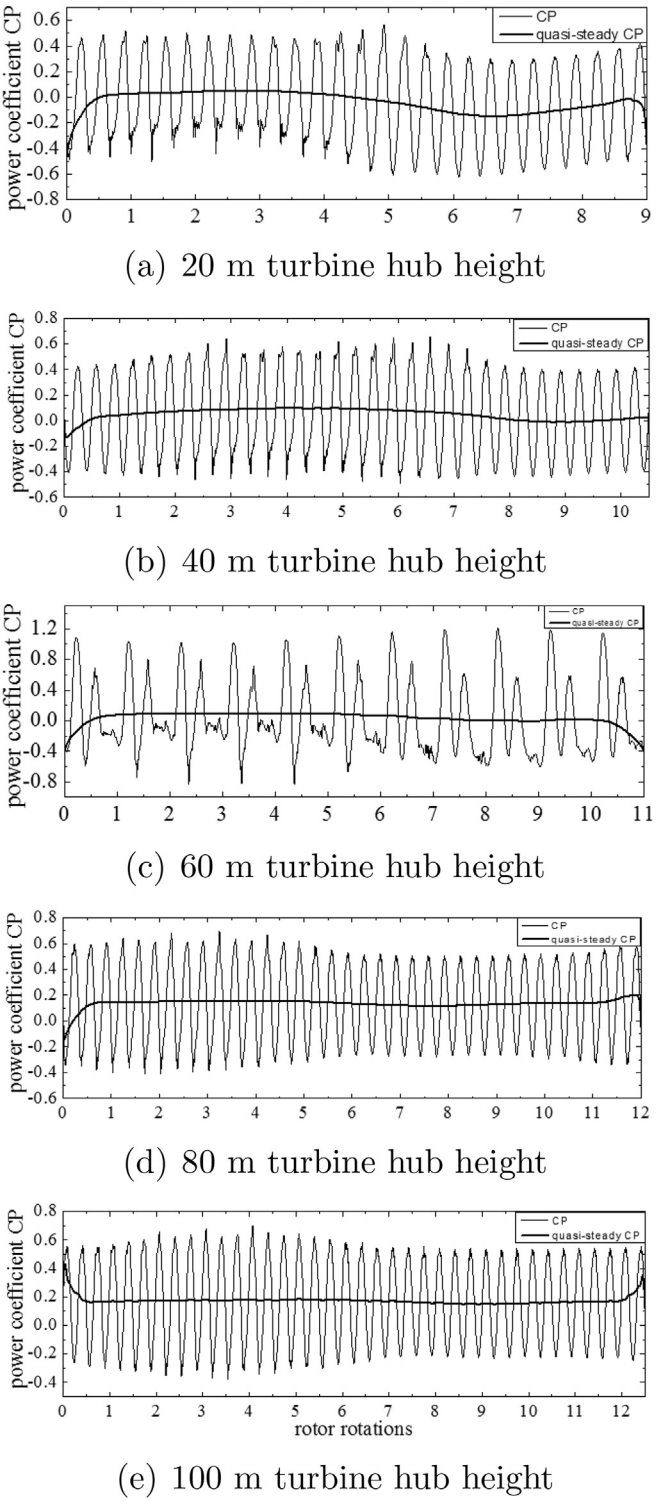


**Fig. 7.** Power coefficient at various turbine hub heights.

turbine operation at a remote power-starved population in rural Kenya. The small wind turbine aerodynamic performances at the site have been analysed at five turbine hub heights. The empirical and numerical wind power densities revealed a similar variation across turbine hub heights for the plateau terrain region, with the numerical method less prone to many statistical errors. Hence, the numerical method is reliable in addressing the SWT aerodynamic performances for the plateau region.

At lowest turbine hub height of 20 m, numerical $P_B$ and $P_w$ are −0.27 W and 31.15 W, respectively, resulting into a negative power coefficient of −0.01. In addition, because of the low wind power density values, 44.50–85.48 W/m$^2$ between turbine hub heights 20 and 60 m, the plateau region corresponds to wind class ≈1; hence, the site is unsuitable for grid-connected power generation. Compared to the prevailing empirical methods, the CFD numerical approach could be considered as an alternative, inexpensive and robust application method for addressing the SWT aerodynamic performance.

The numerical approach considers wind velocity fluctuations at the site without assessing topology effects and the power response of a small wind turbine to wind speed frequency distribution within the regime. Instead, the single frequency numerical model is intended to specifically elucidate the CFD application and its added value with respect to the empirical approach. Therefore, future work will be extended to develop a multiple-frequency-component model to combine multiple frequencies within the wind regime.

## Acknowledgements

This research work was supported in part by the Institute of Dynamics and Control of Spacecrafts, School of Astronautics, through the Harbin Institute of Technology; and the Chinese Scholarship Council, through the People's Republic of China Government (CSC grant no. 2013404003) in collaboration with the Kenyan Government.

## References

[1] O.S. Ohunakin, Wind resource evaluation in six selected high altitude locations in Nigeria, Renew. Energy 36 (2011) 3273–3281.
[2] M. Islam, R. Saidur, N. Rahim, Assessment of wind energy potentiality at Kudat and Labuan, Malaysia using Weibull distribution function, Energy 36 (2011) 985–992.
[3] F. Al-Mansour, B. Sucic, M. Pusnik, Challenges and prospects of electricity production from renewable energy sources in Slovenia, Energy 77 (2014) 73–81.
[4] B. Moreno, A.J. Lopez, M.T. Garcia-Ivarez, The electricity prices in the European Union. The role of renewable energies and regulatory electric market reforms, Energy 48 (2012) 307–313.
[5] B. Mukulo, J. Ngaruiya, J. Kamau, Determination of wind energy potential in the Mwingi-Kitui plateau of Kenya, Renew. Energy 63 (2014) 18–22.
[6] B.K. Sovacool, M. Kryman, T. Smith, Scaling and commercializing mobile biogas systems in Kenya: a qualitative pilot study, Renew. Energy 76 (2015) 115–125.
[7] R.K. Singh, M.R. Ahmed, M.A. Zullah, Y.H. Lee, Design of a low Reynolds number airfoil for small horizontal axis wind turbines, Renew. Energy 42 (2012) 66–76. International Symposium on Low Carbon and Renewable Energy Technology 2010 (ISLCT 2010).
[8] R. Howell, N. Qin, J. Edwards, N. Durrani, Wind tunnel and numerical study of a small vertical axis wind turbine, Renew. Energy 35 (2010) 412–422.
[9] K. Kelly, M. McManus, G. Hammond, An energy and carbon life cycle assessment of industrial CHP (combined heat and power) in the context of a low carbon UK, Energy 77 (2014) 812–821.
[10] J. Zhang, S. Chowdhury, A. Messac, B.-M. Hodge, Assessing long-term wind conditions by combining different measure-correlate-predict algorithms, in: ASME International Design Engineering Technical Conferences, Portland, Oregon, vol. 3A.
[11] A. Kusiak, Z. Zhang, A. Verma, Prediction, operations, and condition monitoring in wind energy, Energy 60 (2013) 1–12.
[12] E. Vladislavleva, T. Friedrich, F. Neumann, M. Wagner, Predicting the energy output of wind farms based on weather data: important variables and their correlation, Renew. Energy 50 (2013) 236–243.
[13] Kenya National Bureau of Statistics, Energy Use in Kitui County, 2009, National population census report, 2010.
[14] D. Theuri, Lead Implementer, Solar and Wind Energy Assessment Report (UNEP-project), Technical Report, SWERA, in: Kenya Country Report, May 23 2008.
[15] A. Pourrajabian, M. Mirzaei, R. Ebrahimi, D. Wood, Effect of air density on the performance of a small wind turbine blade: a case study in Iran, J. Wind Eng. Ind. Aerod. 126 (2014) 1–10.
[16] Y. He, P. Chan, Q. Li, Wind characteristics over different terrains, J. Wind Eng. Ind. Aerod. 120 (2013) 51–69.
[17] P. Sparks, Z. Huang, Gust factors and surface-to-gradient wind-speed ratios in tropical cyclones, J. Wind Eng. Ind. Aerod. 89 (2001) 1047–1058.
[18] S. Cao, Y. Tamura, N. Kikuchi, M. Saito, I. Nakayama, Y. Matsuzaki, Wind characteristics of a strong typhoon, J. Wind Eng. Ind. Aerod. 97 (2009) 11–21.
[19] J. Ashcroft, The relationship between the gust ratio, terrain roughness, gust duration and the hourly mean wind speed, J. Wind Eng. Ind. Aerod. 53 (1994) 331–355.
[20] C. Georgakis, M. Santamouris, On the estimation of wind speed in urban canyons for ventilation purposes-part 1: coupling between the undisturbed wind speed and the canyon wind, Build. Environ. 43 (2008) 1404–1410.
[21] T.-P. Chang, H.-H. Ko, F.-J. Liu, P.-H. Chen, Y.-P. Chang, Y.-H. Liang, H.-Y. Jang, T.-C. Lin, Y.-H. Chen, Fractal dimension of wind speed time series, Appl. Energy 93 (2012) 742–749.
[22] I. Fyrippis, P.J. Axaopoulos, G. Panayiotou, Wind energy potential assessment in Naxos island, Greece, Appl. Energy 87 (2010) 577–586.
[23] W. Zhou, H. Yang, Z. Fang, Wind power potential and characteristic analysis of the pearl river delta region, China, Renew. Energy 31 (2006) 739–753.
[24] J. Seguro, T. Lambert, Modern estimation of the parameters of the Weibull wind speed distribution for wind energy analysis, J. Wind Eng. Ind. Aerod. 85 (2000) 75–84.
[25] J. Kamau, R. Kinyua, J. Gathua, 6 years of wind data for Marsabit, Kenya average over 14 m/s at 100 m hub height; an analysis of the wind energy potential, Renew. Energy 35 (2010) 1298–1302.
[26] D.W. Wekesa, C. Wang, Y. Wei, J.N. Kamau, L.A.M. Danao, A numerical analysis of unsteady inflow wind for site specific vertical axis wind turbine: a case study for Marsabit and Garissa in Kenya, Renew. Energy 76 (2015) 32–45.
[27] D.W. Wekesa, C. Wang, Y. Wei, L.A.M. Danao, Influence of operating conditions on unsteady wind performance of vertical axis wind turbines operating within a fluctuating free-stream: a numerical study, J. Wind Eng. Ind. Aerod. 135 (2014) 76–89.
[28] D.W. Wekesa, C. Wang, Y. Wei, J.N. Kamau, Wind resource assessment and numerical simulation for wind turbine airfoils, in: 2014 15th International Workshop on Research and Education in Mechatronics (REM), Egypt, vol. 15, IEEE, 2014, pp. 1–9.
[29] D.W. Wekesa, J.N. Mutuku, J.N. Kamau, Microcontroller-based data logging instrumentation system for wind speed and direction measurements, J. Agric. Sci. Technol. 14 (2012) 176–189.
[30] L.E.B. Sampaio, A.L.T. Rezende, A.O. Nieckele, The challenging case of the turbulent flow around a thin plate wind deflector, and its numerical prediction by LES and rans models, J. Wind Eng. Ind. Aerod. 133 (2014) 52–64.
[31] L.A. Danao, J. Edwards, O. Eboibi, R. Howell, A numerical investigation into the influence of unsteady wind on the performance and aerodynamics of a vertical axis wind turbine, Appl. Energy 116 (2014) 111–124.
[32] S. Wang, D.B. Ingham, L. Ma, M. Pourkashanian, Z. Tao, Numerical investigations on dynamic stall of low reynolds number flow around oscillating airfoils, Comput. Fluids 39 (2010) 1529–1541.
[33] R. Nobile, M. Vahdati, J.F. Barlow, A. Mewburn-Crook, Unsteady flow simulation of a vertical axis augmented wind turbine: a two-dimensional study, J. Wind Eng. Ind. Aerod. 125 (2014) 168–179.
[34] O. Eboibi, L.A. Danao, R. Howell, J.M. Edwards, A numerical study of the influence of blade profile and solidity on the performance of vertical axis wind turbines, in: 51st AIAA Aerospace Sciences Meeting Including the New Horizons Forum and Aerospace Exposition, 2013.
[35] D. Mehta, A. van Zuijlen, B. Koren, J. Holierhoek, H. Bijl, Large Eddy Simulation of wind farm aerodynamics: a review, J. Wind Eng. Ind. Aerod. 133 (2014) 1–17.
[36] H. Aboshosha, G. Bitsuamlak, A. El Damatty, Turbulence characterization of downbursts using LES, J. Wind Eng. Ind. Aerod. 136 (2015) 46–61.
[37] P. Warzecha, A. Boguslawski, LES and RANS modeling of pulverized coal combustion in swirl burner for air and oxy-combustion technologies, Energy 66 (2014) 732–743.
[38] D. Allaei, Y. Andreopoulos, Invelox: description of a new concept in wind power and its performance evaluation, Energy 69 (2014) 336–344.
[39] S. McIntosh, H. Babinsky, T. Bertenyi, Optimizing the energy output of vertical axis wind turbines for fluctuating wind conditions, in: 45th AIAA Aerospace Sciences Meeting and Exhibit, Reno, Nevada.
[40] S. McIntosh, H. Babinsky, T. Bertenyi, Unsteady power output of vertical axis wind turbines operating within a fluctuating free-stream, in: 46th AIAA Aerospace Sciences Meeting and Exhibit, Reno, Nevada.
[41] F. Scheurich, R.E. Brown, Modelling the aerodynamics of vertical-axis wind turbines in unsteady wind conditions, Wind Energy 16 (2013) 91–107.
[42] A.M. Abdelsalam, K. Boopathi, S. Gomathinayagam, S.H.K. Kumar, V. Ramalingam, Experimental and numerical studies on the wake behavior of a horizontal axis wind turbine, J. Wind Eng. Ind. Aerod. 128 (2014) 54–65.
[43] M. Raciti Castelli, A. Englaro, E. Benini, The Darrieus wind turbine: proposal for a new performance prediction model based on CFD, Energy 36 (2011) 4919–4934.
[44] S.M. Mortazavi, M.R. Soltani, H. Motieyan, A pareto optimal multi-objective optimization for a horizontal axis wind turbine blade airfoil sections utilizing exergy analysis and neural networks, J. Wind Eng. Ind. Aerod. 136 (2015) 62–72.
[45] V. D'Alessandro, S. Montelpare, R. Ricci, A. Secchiaroli, Unsteady aerodynamics of a Savonius wind rotor: a new computational approach for the simulation of energy performance, Energy 35 (2010) 3349–3363.
[46] L.A. Danao, O. Eboibi, R. Howell, An experimental investigation into the influence of unsteady wind on the performance of a vertical axis wind turbine,

Appl. Energy 107 (2013) 403–411.
[47] J.M. Edwards, L.A. Danao, R.J. Howell, Novel experimental power curve determination and computational methods for the performance analysis of vertical axis wind turbines, J. Sol. Energy Eng. 134 (2012) 031008.
[48] S. McTavish, D. Feszty, T. Sankar, Steady and rotating computational fluid dynamics simulations of a novel vertical axis wind turbine for small-scale power generation, Renew. Energy 41 (2012) 171–179.
[49] M. Moshfeghi, Y.J. Song, Y.H. Xie, Effects of near-wall grid spacing on SST-k-w model using NREL phase VI horizontal axis wind turbine, J. Wind Eng. Ind. Aerod. 107–108 (2012) 94–105.
[50] P.C. Rocha, H.B. Rocha, F.M. Carneiro, M. Vieira da Silva, A.V. Bueno, k-w SST (Shear Stress Transport) turbulence model calibration: a case study on a small scale horizontal axis wind turbine, Energy 65 (2014) 412–418.
[51] L.A. Danao, N. Qin, R. Howell, A numerical study of blade thickness and camber effects on vertical axis wind turbines, Proc. Inst. Mech. Eng. Part A J. Power Energy 226 (2012) 867–881.
[52] R. Nobile, M. Vahdati, J.F. Barlow, A. Mewburn-Crook, Unsteady flow simulation of a vertical axis augmented wind turbine: a two-dimensional study, J. Wind Eng. Ind. Aerod. 125 (2014) 168–179.
[53] S. Mcintosh, Wind Energy for the Built Environment, PhD Thesis, Department of Engineering, Cambridge University, 2009, pp. 105–106, 164.
[54] National Renewable Energy Laboratory (NREL), Wind Data Details: http://www.nrel.gov/gis/wind_detail.html, (accessed 01.11.15).